J Solid State Electrochem
DOI 10.1007/s10008-012-1966-2

ORIGINAL PAPER

Pt||ZrO_2 nanoelectrode array synthesized through the sol–gel process: evaluation of their sensing capability

Jadra Mosa · Adrián Carretero-Genevrier · David Grosso · Christel Laberty-Robert · Clement Sanchez

Received: 14 October 2012 / Revised: 26 November 2012 / Accepted: 29 November 2012

Abstract Homogeneous, circular Pt||ZrO_2 nanoelectrodes have been synthesized through the sol–gel chemistry and the dip-coating process. These nanoelectrode arrays have been evaluated as a platform for electropolymerization of phenol, as model. We have shown that the microstructure of the polymer depends on the confined environment of the electrode and on the position of the –OH group of the monomer. Additionally, these nanoelectrodes have been tested as an electrochemical sensor for dihydroxybenzene isomers in aqueous medium. These Pt||ZrO_2 nanoelectrodes exhibit a detection limit of 2×10^{-7}M for resorcinol and 1×10^{-6}M for catechol.

Keywords Pt||ZrO_2 nanoelectrode arrays · Electrochemical sensor · Dihydroxybenzenes · Sol–gel chemistry · Selective determination

Introduction

Dihydroxybenzenes (such as catechol and resorcinol) are widely used in industrial processes, such as photography, dye, cosmetic, chemical, and pharmaceutical industries [1]. Elevated levels of phenolic compounds constitute a substantial risk to the natural environment because they are absorbed by animals and humans through the skin and the mucous membranes. As a large variety of phenolic compounds exists, they show a broad range of toxicity levels, affecting a large variety of organs and tissues [2].

Analytical methods for the detection and quantification of mixtures of phenols are based on separation techniques, allowing the identification and quantification of individual constituents. Moreover, techniques such as chromatography, fluorimetry, and spectrometry are expensive, time-consuming, and require pre-concentration and extraction steps that increase the risk of sample loss or contamination [3]. To overcome these inconveniences, electrochemical sensors based on carbon electrodes have been recently developed [4]. They provide low detection limits, a wide linear response range, and a good stability and reproducibility [5]. The detection limit is in the micromole to millimole range depending on the nature of the carbon, i.e., glassy carbon, carbon nanotubes (CNTs), or array of carbon nanotubes. However, the carbon electrodes made of CNTs are quite expensive and are mainly dedicated to specific applications [5]. Recently, several authors reported sensors and biosensors showing great promise for a rapid, highly sensitive, and simple analysis of polyphenols. Compositions are diverse, mainly based on glassy carbon electrodes or carbon nanotubes or mixtures, with additives such as Nafion, ionic liquids, or biologic molecules [6–12].

In the literature, electrochemical sensors based on Pt electrode have been reported. To our knowledge, bare Pt electrodes exhibit high sensibility to pollutant contamination which impact their stability and efficiency with time and poor selectivity [13, 14]. The modification of this electrode in order to improve their sensibility and selectivity through a nanostructuration of their surface represents an interesting approach [15]. In this paper, we adopt a different strategy to increase their sensibility and to improve their

J. Mosa · A. Carretero-Genevrier · D. Grosso · C. Laberty-Robert (✉) · C. Sanchez
Laboratoire Chimie de la Matière Condensée de Paris (UMR 7574), Collège de France–Université Pierre et Marie Curie–CNRS, Collège de France, Bat. C-D, 11 Place Marcelin Berthelot, 75231 Paris, France
e-mail: christel.laberty@upmc.fr

J. Mosa
Instituto de Cerámica y Vidrio (CSIC), C/ Kelsen 5 (Campus de Cantoblanco), 28049 Madrid, Spain

Published online: 20 December 2012

selectivity by creating an array of Pt nanoelectrodes [15–20]. To do this, we propose to pattern the surface of a thin Pt layer deposited on silicon wafer with a well-defined thin, porous ZrO_2 layer. These Pt nanoelectrode arrays can be described as Pt nanoholes with a well-defined diameter, dispersed onto silicon substrates. Inorganic, insulating ceramic separates these nanoholes. The distance between two Pt disks and their diameters depend on both the sol–gel chemistry and the dip-coating process [17]. Because the inorganic porous layer is stable in various pH conditions (isoelectric point for ZrO_2, pH=9), these electrodes are versatile and robust. Additionally, careful control of the synthesis conditions allows the synthesis of Pt nanoelectrode arrays exhibiting a stationary response. This corresponds to Pt nanoelectrodes with a radius of 8 nm and a 240-nm distance between two electrodes when interelectrode distance, d, and the diameter of the electrode, r, keep a ratio of $d>12r$ [21]. An amplification of the current occurs with hysteresis as a separation of the forward and reverse cyclic voltammetry (CV) scan is observed. This indicates a high capacitive current [21]. Unfortunately, these conditions are indicative of poor sealing of the ceramic layer on the Pt film. For other sol–gel chemistry and dip-coating conditions, these Pt nanoelectrode arrays behave as macroelectrode ($d<12r$), in which the individual diffusion fields of the Pt nanoelectrode emerge to form a linear diffusion regime. However, depending on the scan rates, these Pt nanoelectrode arrays may have different mass transport that will modify their selectivity and reactivity [20]. Macroelectrode with a well-defined hierarchical pore system would present a good compromise, ensuring very fast mass transport properties with ultrahigh active surface areas [22]. In this paper, we have tested these Pt nanoelectrode arrays, when a macroelectrode behavior is observed, as a sensor. We have reported the sensibility and the capability of these Pt||ZrO_2 nanoelectrodes for the quantification and the separation of phenolic compounds through pulse voltammetry (DPV) method. In parallel, we have modified these Pt nanoelectrode arrays through the electrochemical polymerization of different monomers (catechol and resorcinol, designed as polyphenol oxide (PPO)). This study was performed in order to synthesize Pt nanoelectrode arrays, on top of which semi-permeable membranes are electrodeposited. This might open the field to semi-permeable nanoelectrode arrays exhibiting different selectivity and sensibility.

Experimental

Synthetic procedures

ZrO_2 mesostructured thin films were synthesized as previously reported [20]. Nanoelectrode arrays were synthesized from zirconium oxide nanoperforated membranes deposited on a conductive platinum layer on Si(001) substrates (Si-Tech, Inc.). The process involved nanotexturation of a surface through solution deposition of zirconia precursors using *block* copolymer micelles, followed by a short thermal treatment in air. Solution A consisted of polybutadiene-*b*-polyethylene oxide (PB-*b*-PEO; MW_{PB}=5,500 g·mol^{-1}, MW_{PEO}=30,000 g·mol^{-1} (Polymer Source, Inc.)), EtOH (4.5 g; absolute ethyl alcohol, Normapur), and water (0.2 g). Solution A was placed in a drying oven at 70 °C until the copolymer PB-*b*-PEO was completely dissolved, and then it was left at room temperature to equilibrate. Solution B, made of $ZrCl_4$ (100 mg, Cl>98 %; Fluka AG) and EtOH (1.5 g), was added to solution A. The final sol–gel solution C was stirred for 30 min at room temperature for homogenization. ZrO_2-based films were elaborated by dip-coating the Pt/Si(001) substrates into the sol–gel solution C at a constant withdrawal speed of 0.3 mm·s^{-1} under a constant temperature of 70 °C and controlled relative humidity (<2 %). The films were directly heated at 450 °C for 15 min under static air to complete the inorganic condensation of the matrix and to decompose the *block* copolymer template.

Optimization of electropolymerization conditions

Electrolyte solution was selected according to the solubility conditions of the monomers. Catechol was soluble in organic solvents. Its solubility decreases in water, but it is maintained in basic pH. In contrast, resorcinol is highly soluble in water, and its solubility decreases in organic solvents. In order to compare both monomers, an aqueous basic solution was chosen [21–23]. Different potential ranges for catechol and resorcinol were selected in order (1) to avoid secondary reactions and (2) to promote polymerization. A potential maximum of +1 and +0.6 V for catechol and resorcinol, respectively, was chosen to carry out the polymerization of the PPO films by cyclic voltammetry. This potential is high enough to deposit a considerable amount of polymer at each cycle. High potentials were avoided because usually they produce polymer degradation because the medium is aqueous [22–24]. In order to choose the adequate scan rate for the cyclic voltammetry experiments, several cycles were performed for catechol and resorcinol at various scan rates of 20, 50, and 100 mV s^{-1}. For catechol, the height of the anodic peak is gradually decreased when the number of PPO deposition cycles increases. This indicates that the electrochemically active area of the electrodes decreases with the polymer loading. For resorcinol with a scan rate of 100 mV s^{-1}, the response compares well with the one observed for catechol. However, the intensity of the main peak increases when increasing the number of cycles at low scan rates (20 mV s^{-1}), probably due to the existence of a secondary

reaction (oxidation or dissolution of the polymer). Thus, a scan rate of 50 mV s^{-1} has been chosen.

Finally, the polymer film thickness can be tuned by changing the monomer concentration or the number of cycles [21, 24]. For 10 cycles, when changing the monomer concentration range from 3 to 20 mM, an increase of the intensity of the anodic voltammetric peak is observed up to 12 mM for cathechol and 10 mM for resorcinol. Then, the intensity of the peak remained constant. Summarizing, selected conditions for electropolymerization were as follows: maximum potentials of +1 V (catechol) and +0.6 V (resorcinol), scan rate of 50 mV s^{-1}, and monomer concentration of 12 mM.

Preparation of Pt-modified electrode

The poly(catechol) and poly(resorcinol) (PPO films) were electrodeposited from an electrolyte (pH=basic) consisting of 0.10 M of sodium hydroxide and 12 mM of monomer source (catechol or resorcinol) in water solution (all of them purchased from Aldrich). The working electrode, Pt||ZrO_2 nanoelectrode, was placed in a standard three-electrode cell consisting of a Pt wire as the counter electrode and a saturated calomel electrode (SCE) as the reference with a potential of −241 mV vs H_2. A potentiostat galvanostat (Princeton Applied, 262) was used for the electrosyntheses and voltammetric measurements. The different PPO films were electrodeposited on the Pt||ZrO_2 working nanoelectrode array using −0.6 and 1 V vs SCE for catechol and −0.2 and 0.6 V for resorcinol up to 30 cycles at a sweep rate of 50 mV s^{-1}. For all the electrochemistry experiments, the geometrical surface working electrode is 0.192 cm^2. The PPO-coated Pt||ZrO_2 nanoelectrode array (PPO||Pt||ZrO_2) was rinsed with deionized water and dried with argon.

Thin-film characterization

Image processing was done using Gwyddion software (http://gwyddion.net), which is a modular program for scanning probe microscopy, for data visualization and analysis. To further clarify the structural arrangement of the ZrO_2 nanocraters, the normalized surface autocorrelation function corresponding to the topological atomic force microscopy (AFM) image shown in Fig. 1b has been calculated (Fig. 1c). The height–height correlation function is defined as $C(r) = \langle [z(r_0 + r) - \langle z \rangle][z(r_0) - \langle z \rangle] \rangle$, where $m\langle z \rangle$ means the average over all possible pairs in the matrix that are separated by a vector r from the center of an image given by the vector r_0, and z values are the deviation from the average height $\langle \ldots \rangle$ [25]. NEA surface topography and nanostructure were deduced from AFM investigations using a Veeco DI-CPII in non-contact mode using MPP11120 etched silicon probes from Veeco. Scanning electron micrographs were obtained on a scanning electron microscope equipped with a field emission gun (JEOL 6500 F) using an accelerating voltage of 5 kV and a magnification of 8,000–15,000. As the substrate is an electronic conductor, the uncoated and PPO-coated Pt||ZrO_2 electrodes were analyzed as received. To understand the formation of catechol or resorcinol films onto the Pt nanoelectrodes, Fourier transform infrared (FTIR) spectra were performed on a Perkin Elmer Spectrum 100 spectrometer in the range 1,550–1,300 cm^{-1} using a transmittance mode with a resolution of 2 cm^{-1}. Cyclic voltammetry experiments were performed in a three-electrode cell with a SCE reference electrode and a Pt wire counter electrode, using a geometrical surface working electrode area of 0.192 cm^2 in monomer solutions. The electrochemical parameters for DPV were optimized at a scan rate of 200 mV s^{-1} (a fast scan rate was chosen because a mixed regime in response to the Pt nanoelectrode arrays was observed [21]), 30-mV pulse amplitude, and 50-ms pulse width. All the electrochemical experiments were performed at room temperature.

Results and discussion

Synthesis and characterization of Pt nanoelectrode arrays

The ZrO_2 porous layer is thin and exhibits a hexagonal array of nanoholes with a diameter of 40 nm and a center-to-center distance of 80 nm. The typical morphology of Pt||ZrO_2 nanoelectrodes is shown in Fig. 1a. AFM images show well-dispersed in-plane circular shape motifs surrounded by ZrO_2 inorganic matrices. A topological AFM image (Fig. 1b) offers a deeper insight into the arrangement of the nanoholes. These nanoholes defined Pt nanoelectrodes. The distance between the nanoholes is shown in the 2D fast Fourier transform (FFT). Six dots with high intensity are clearly identified, demonstrating that the nanoholes are regularly arranged along three specific directions. The center-to-center distance changes from 50 to 80 nm. The diameter of the Pt nanodisk (or the nanoholes) is d=40±1.0 nm. To further clarify the structural arrangement of the ZrO_2 nanocraters, the normalized surface autocorrelation function corresponding to the topological AFM image shown in Fig. 1b has been calculated (Fig. 1c). A clear distorted hexagonal pattern appears, indicating that the Pt nanodisks or Pt nanoelectrodes are regularly arranged on the overall surface. Figure 1d shows profiles of the autocorrelation function in both diagonal l_D and parallel $l_{//}$ directions to the analyzed distortion in the Pt nanoelectrode hexagonal pattern. In both directions, intense peaks (number 10) are observed. No vanishing oscillations are observed at large distances, indicating the existence of a large-range order in the Pt nanoelectrode networks. This confirmed the 2D FFT

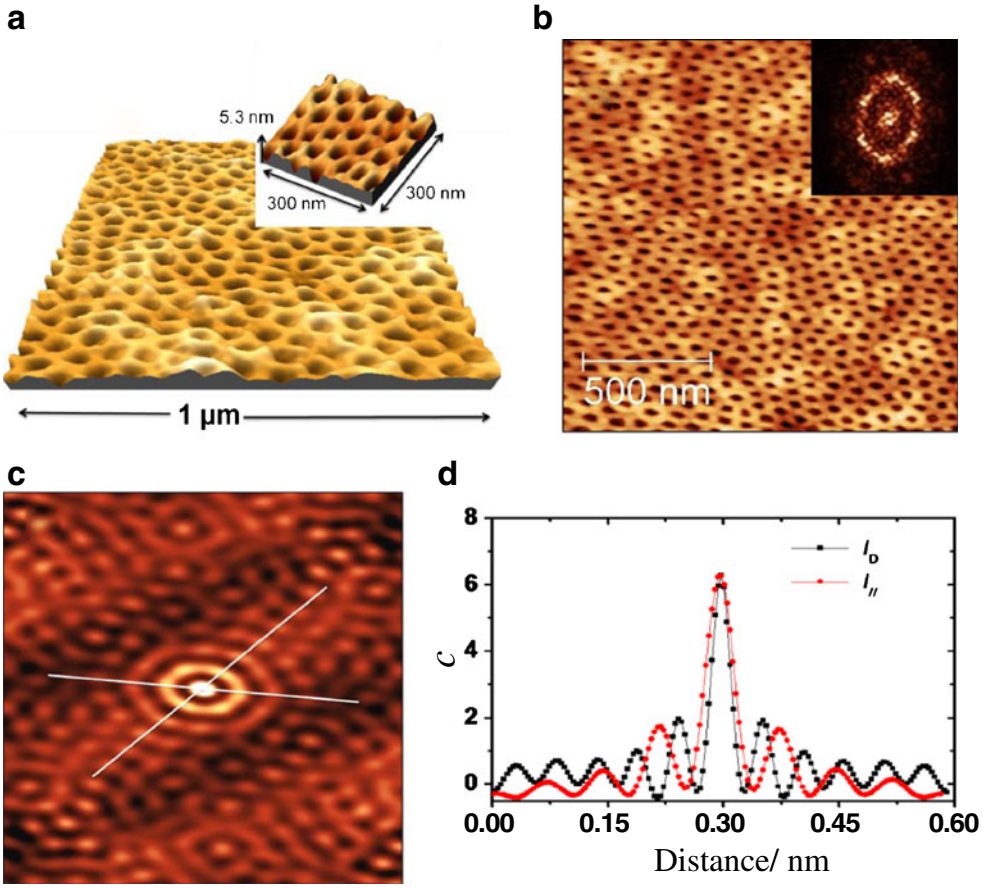

Fig. 1 AFM images showing the topography of Pt||ZrO_2 nanoelectrodes at different magnifications (**a** and **b**). *Inset* shows the 2D FFT of the topographic image, showing the distance between the periodic motifs. **c** AFM image of the close-packed assemblies of nanoholes or Pt nanodisks. **d** Autocorrelation functions of the topographic image shown in Fig. 1c with the corresponding profiles along the *white lines*

results. The average distance between Pt||ZrO_2 nanoelectrodes was l_D 53 nm and $l_{//}$ 76 nm, which agrees with the values obtained from the 2D FFT. Accordingly, the hole density, a, is evaluated to be 9.5×10^9 electrodes cm^{-2}. The accessibility of the Pt surface area is then estimated to be 0.40 cm^2 for 1 cm^2 of macroelectrode. The 12-nm thickness of the ZrO_2 ceramic was measured from cross-section SEM images and reflectometry analyses (not shown) [14, 21]. These nanoelectrodes have been used as platform for the electrochemical polymerization of dihydroxybenzene isomers.

Pt nanoelectrode arrays as platform for electropolymerization

We examined the electropolymerization of different phenol isomers, catechol and resorcinol. We used them as a model to study whether the ZrO_2 ceramic onto the Pt substrates affects the electropolymerization mechanisms. Based on literature data [26–28], the electropolymerization of PPO films was done in basic medium through cyclic voltammetry experiments in different potential ranges in order to avoid secondary reactions and dissolution of the PPO film [22, 23, 29]. Figure 2a shows typical electropolymerization curves for cathechol. During the first cycle, a sharp anodic oxidation peak (Ep=0.2 V) is observed, corresponding to the oxidation of the phenoxide anion to a phenoxy radical. The size of the reduction peak is smaller than that of the anodic peak, suggesting a quasi no-reduction peak [22, 30]. The height of the oxidative peak decreases with the number of cycles, indicating a passivation of the electrode. Passivation was completed after 30 cycles as a small current on the CV curves was observed. Figure 2b shows the voltammetric behavior of resorcinol that differs from the one observed for cathechol. This change is mainly related to the difference in reactivity of the –OH groups onto the aromatic ring. More precisely, –OH groups in *ortho*- and *para*- positions are more reactive than the one localized in the *meta*- position [30–32]. Resorcinol polymerization then occurs at higher potential (+0.25 V vs SCE), and its intensity is low due to the presence of enolic form that is not generated after the different cycles.

Pt||ZrO_2 nanoelectrode arrays after polymerization of phenol were examined through SEM analyses. Figure 3 presents SEM images obtained for catechol for two different conditions of polymerization: (a) 3 cycles and (b) 30 cycles. We can see that after 30 cycles, the Pt nanoelectrodes are selectively covered by the polymer. For resorcinol, polymerization is much faster; the Pt nanoelectrodes were covered with polymer after 20 cycles (Fig. 3d). The morphology and

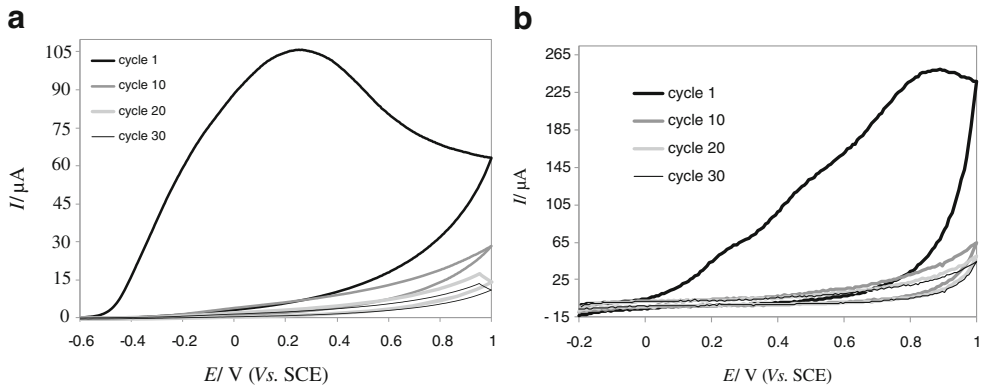

Fig. 2 Cyclic voltammetry of catechol on Pt||ZrO_2 nanoelectrodes as a function of the number of cycles. **a** Catechol and **b** resorcinol (monomer concentration of 12 mM)

the kinetic of growth of the poly(resorcinol) and poly(catechol) films onto the Pt nanoelectrodes depend on the nature of the monomer, more precisely on the position of the –OH groups onto the phenolic ring. A highly branched polymer is observed for resorcinol due to the distance between the –OH group (1,3 dihydroxy), while a dense film is formed for catechol [32]. This is related to its polymerization in a linear mode [33–35]. In contrast, a different electropolymerization rate was observed for the bare electrode. The kinetic of resorcinol growth is lower when the electropolymerization occurs on the flat surface because of the low reactivity of the –OH group onto the metal position. This effect can be explained by a competition between lowering the surface energy and minimizing the entropy of the polymer chains, in which their respective ratio may be modified through confinement effect [36].

FTIR analyses were then used to analyze the as-synthesized films onto the Pt||ZrO_2 nanoelectrode array and to follow the polymerization rate. Previous results have shown that the nature of the electrode influences the polymerization rate as the interaction with the active surface differs [37, 38]. FTIR spectra (Fig. 4) show that cathechol is attached to the surface via catecholate monodentate [39–43] as $\nu_{C=C}$ vibration band shifts to the red (24 cm^{-1}) after 3 cycles. These bands do completely disappear after 30 cycles. In contrast, the δ_{OH} band shifts towards higher wave numbers from 1,364 to 1,384 cm^{-1} which indicates an electrodonation mechanism. For resorcinol, the FTIR spectra exhibit a slight modification of the $\nu_{C=C}$ vibration bond and a disappearance of the δ_{OH} band after 3 cycles. This indicates that (1) resorcinol interacts with the substrate via hydrogen bond and (2) the polymerization rate is fast [40–42, 44, 45]. Note that similar experiments were performed on flat Pt electrodes. Differences have been found in terms of polymerization rate and the microstructure of the polymer achieved. This work indicates that a hybrid organic/inorganic platform can be synthesized through a bottom-up approach. These Pt||ZrO_2 nanoelectrodes can be used as nanoreactors to grow polymer films. The rate of polymerization depends on the position of the –OH group. Because this electropolymerization occurs in a confined environment, the microstructure of the polymer is modified.

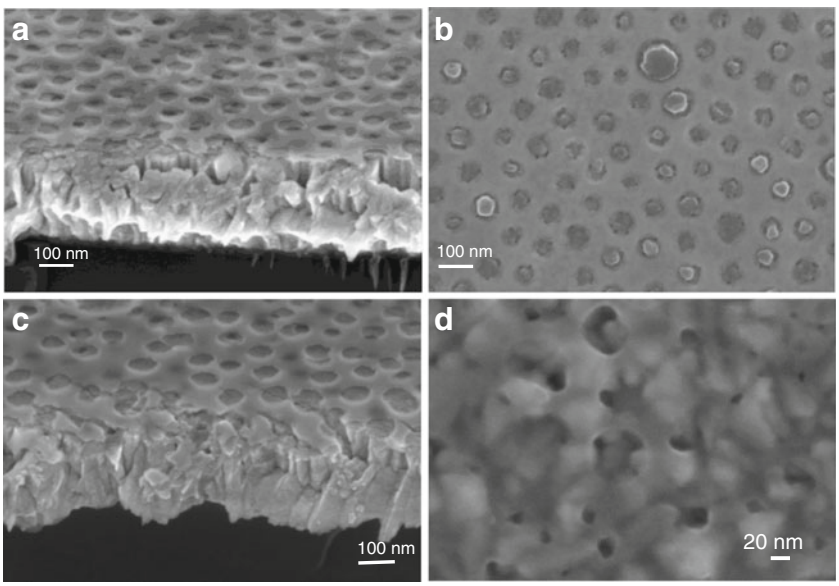

Fig. 3 SEM micrographs for resorcinol after 3 (**a**) and 20 cycles (**b**) and catechol after 3 (**c**), and 30 cycles (**d**)

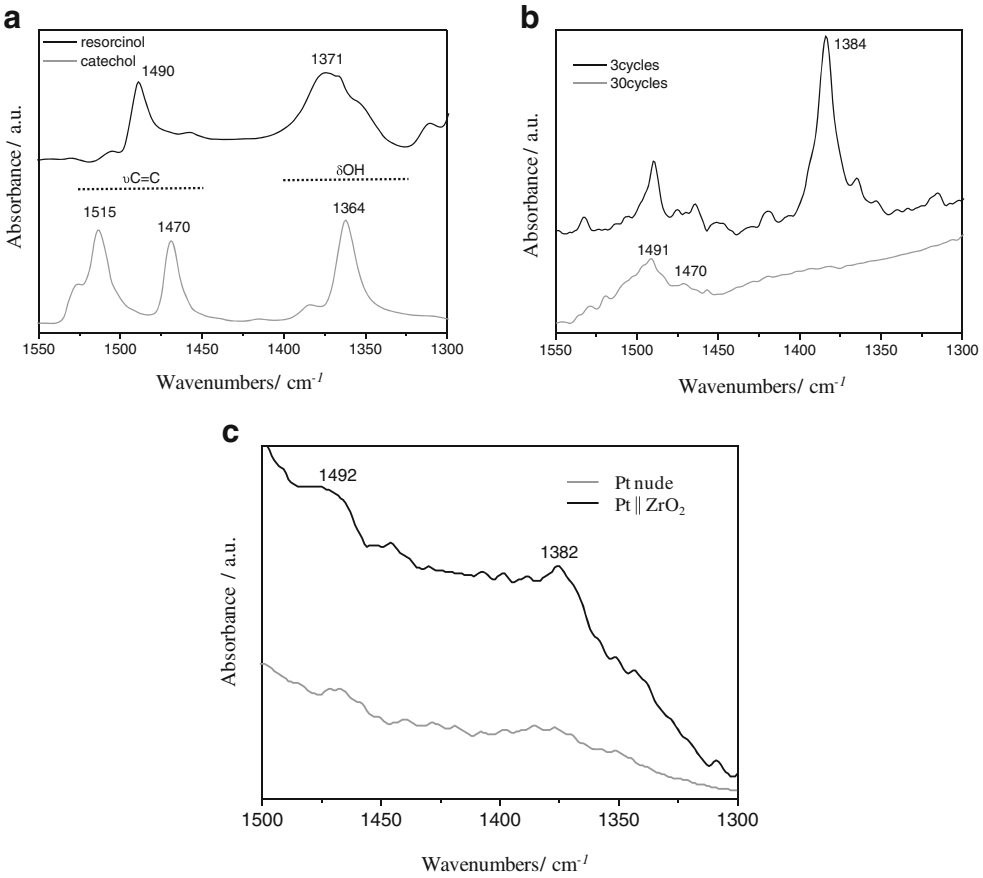

Fig. 4 FTIR spectra of **a** catechol and resorcinol (as purchased). **b** Catechol and **c** resorcinol interactions for Pt||ZrO_2 nanoelectrode after 3 cycles and Pt||ZrO_2 nanoelectrode after 30 cycles in the regions 1,550 and 1,300 cm^{-1}

Pt nanoelectrode arrays as electrochemical sensors

We then investigated the potential application of these Pt-modified electrodes as electrochemical sensors. We studied their reactivity toward toxic pollutants such as catechol and resorcinol. Figure 5 shows the cyclic voltammograms of 0.25 mM of catechol in the presence of the same amount of resorcinol on bare Pt electrode and on Pt||ZrO_2 nanoelectrodes. It can be seen that in both cases it is possible to distinguish two well-separated oxidation peaks (ΔEp (bare Pt)=0.75 V, ΔEp (Pt||ZrO_2 nanoelectrodes)=0.66 V). Compared to the bare Pt electrode, the peaks are well defined and intense for the Pt||ZrO_2 nanoelectrode arrays. In these conditions of analyses, these Pt||ZrO_2 nanoelectrode arrays exhibit excellent sensitivity and selectivity toward dihydroxybenzene compared to bare Pt electrode. The results indicated that dihydroxybenzene isomers were separated absolutely using Pt||ZrO_2 nanoelectrodes and could be used as electrochemical sensors.

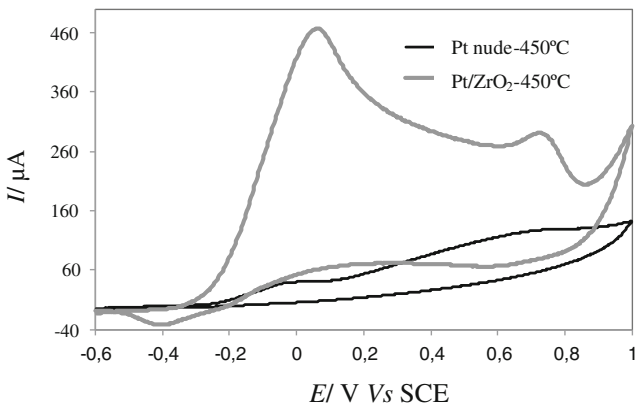

Fig. 5 Cyclic voltammograms of catechol with resorcinol in 0.1 M NaOH containing 0.25 mM catechol and 0.25 mM resorcinol in 0.1 M NaOH on bare electrode and Pt||ZrO_2 nanoelectrode (scan rate 50 mV/s)

DPV method was used for the simultaneous determination of catechol and resorcinol at the sensor (Pt||ZrO_2 nanoelectrodes). The calibration experiments were carried out by varying the concentration of one isomer in the presence of the other. Figure 6a shows the DPV curves of different concentrations of resorcinol in the presence of catechol at a concentration of 5×10^{-4} molL^{-1}. The intensity of the cathodic peak of catechol increased linearly with the catechol concentration (inset in Fig. 6a), while the intensity of the peak corresponding to resorcinol is constant without any mutual interference. The regression equation was I(nA)= 0.018 C (mM)+0.008 (r^2=0.996) in the range 1×10^{-6} – 5×10^{-4} molL^{-1} (Fig. 6b). Similarly, as shown in Fig. 5b, the peak current increased linearly with the increasing of catechol concentration in the range 1×10^{-5} to 4×10^{-4}

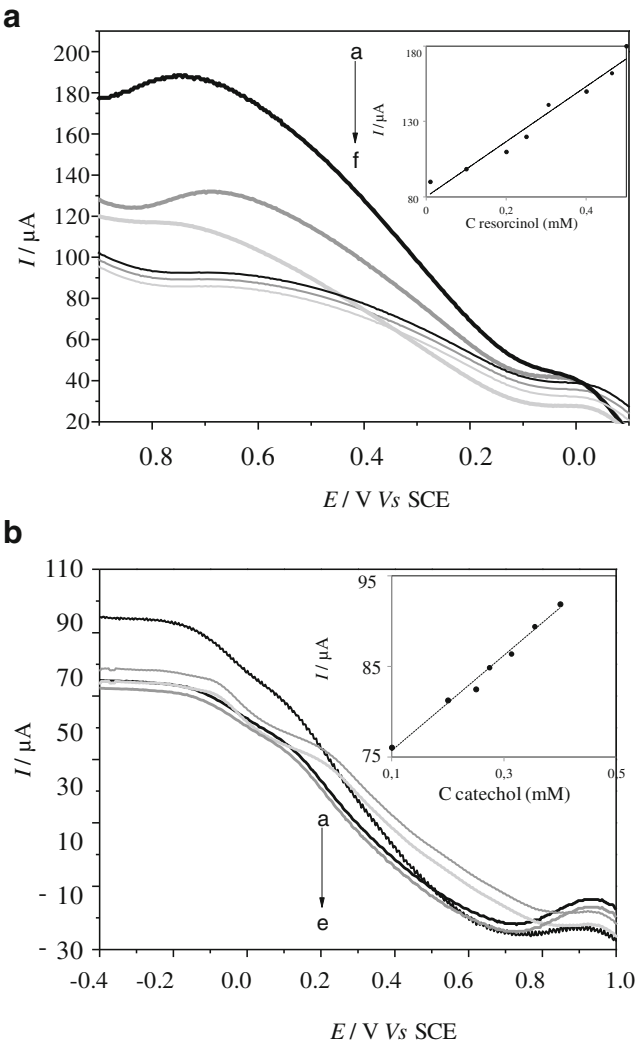

Fig. 6 Differential pulse voltammograms of **a** resorcinol at different concentrations in the presence of 0.5 mM catechol and **b** catechol at different concentrations in the presence of 0.5 mM resorcinol at Pt|| ZrO_2 nanoelectrode. *Inset* shows the relationship between the anodic peak current and the concentration of catechol and resorcinol, respectively. Concentrations: *a* 0.5, *b* 0.4, *c* 0.25, *d* 0.2, *e* 0.1, *f* 0.01 mM

$molL^{-1}$. The regression equation was I(nA)=0.0005 C (mM)+5×10^{-6} (r^2=0.9978). The detection limit was estimated to be 2×10^{-7}M for resorcinol and 1×10^{-6} M for catechol (S/N=3). Measurements of standard samples were carried out three times with relative standard deviations of 3.83 % for catechol and 6.21 % for resorcinol. Catechol and resorcinol exhibited an excellent record with the signal height of the other isomer remaining constant.

The analytical performances of the proposed method were compared with other modified electrodes reported in the literatures [1–12, 15, 41, 46–52]. Results were all summarized in Table 1. The proposed method showed similar electrocatalytic activities toward simultaneous determination of dihydroxybenzene isomers with wider linear range and similar detection limit. This indicates that these Pt||ZrO_2 nanoelectrodes detect independently the different dihydroxybenzenes. This result points out that the proposed method was reliable for the simultaneous and quantitative determination of catechol and resorcinol. The Pt||ZrO_2 nanoelectrode can be modified through the electrodeposition of polymer and exhibit a semi-selective behavior. This polymer electrodeposited inside the nanoelectrodes can selectively allow certain molecules to diffuse toward the membrane. The molecule diffusing throughout the polymer will be

Table 1 Comparable methods for the determination of dihydroxybenzene isomers

Electrodes	Component	Linear range (μM)	Detection limit (μM)	References
GCE/MWCNTs	CC/ RC	2–100 5–80	0.6 1	[1]
GCE/MWCNTs	CC	0.6–100	0.2	[2]
GCE/LDHf	CC	150–3.0	0.1	[3]
PBPB/CNT	CC/RC	1–100	0.3	[4]
MWCNTs	CC/ RC	1–100 6–100	0.2 0.6	[5]
Hb/Cu_2S NRs/ Nafion/GCE	CC/ RC	7–110 8–100	0.5 0.6	[6]
MWCNT/DTDAB/ Tyr/Nafion	CC	2.0–15.0	0.9	[7]
GCE/CNT	CC	1–3.67	1.47	[8]
MWCN/PPO/ AEP/GNPs	CC	1–500	0.8	[9]
Carbon/ILs	CC/ RC	0.5–200 3.5–15.35	0.05 0.5	[10]
GCE/PDDA-G	CC	1–400	0.2	[11]
Graphene/chitosan	CC/ RC	1–400 1–550	0.75 0.75	[12]
Carbon/ mesostructured TiO_2	CC	1–0.02	–	[15]
Mesoporous Pt	CC	1	–	[41]
MWCNT	CC	1–1000	0.6	[46]
CMK-3/GCE	CC	0.5–35	0.1	[47]
ACBK/MWCNT	CC/ RC	1–100 1–100	0.1 0.09	[48]
MWNT/GCE	CC	0.6–100	0.2	[49]
SWNTs	CC/ RC	0.4–10 40–100	0.26 0.3	[50]
Carbon fibers	CC	100–600	–	[51]
NH_2-SBA-15/ carbon	CC/ RC	1–140 2–160	0.5 0.8	[52]

CC catechol, *RC* resorcinol, *GCE* glassy carbon electrode, *MWCNT* multiwall carbon nanotube, *LDHf*, Zn/Al layered double hydroxide, *PBPB* polybromophenol blue, *CNT* carbon nanotubes, *Hb* hemoglobin, *NRs* nanorods, *DTBAD* decylammonium bromide, *Tyr* tyrosinase, *PPO* polyphenol oxidase, *AEP* acetone-extracted propolis, *GNPs* gold nanoparticles, *ILs* ionic liquids, *PDDA-G* diallyldimethylammonium chloride, *CMK-3* mesoporous carbon material, *ACBK* acid chrome blue K, *SWNTs* single-wall carbon nanotube

highly dependent on the nature of the polymer. These molecules can then react with the surface of Pt and allow their detection. The simple sensor exhibited excellent catalytic activity in dihydroxybenzene isomers. The method developed in this study was simple, rapid, and accurate, and it could be applied in the analysis of real samples.

Conclusions

This work proposes an interesting bottom-up approach to fabricate Pt||ZrO_2 nanoelectrode arrays. These Pt||ZrO_2 nanoelectrode arrays are constituted of Pt nanoholes (diameter=40 nm and center-to-center distance=80 nm) surrounded by an insulating, dense ceramic ZrO_2. These Pt||ZrO_2 nanoelectrode arrays have been used to selectively polymerize film onto the Pt surface. Electrodes can then be modified, and original hybrid organic–inorganic nanoelectrodes have been achieved for designing semi-selective electrodes. These Pt nanoelectrode arrays have been tested as sensor for catechol and resorcinol compounds. They exhibit better sensibility and selectivity toward the detection of dihydroxybenzene compared to bare Pt electrode. Because of the stability of the ZrO_2 layer in a wide range of conditions, the method can be applied in medicine, food detection, and environmental control with multi-component analysis.

Acknowledgments The authors are grateful to FCT and Programa Operacional Factores de Competitividade for the financial support (PTDC/CTM/98130/2008). They also acknowledge the Exchange Cooperation Program CNRS/FCT. JM acknowledges the CNRS and Spanish Ministry of Education for the financial support (EX-2009-0671). We acknowledge S. Borensztajn (L.I.S.E–UPR 15 CNRS) for assistance in the SEM characterizations.

References

1. Ding YP, Liu WL, Wu QS, Wang XG (2005) J Electroanal Chem 575:275–280
2. Qi H, Whang C (2005) Electroanalysis 17(10):832–838
3. Li M, Ni F, Wang Y, Wu S, Wang D, Chen S, Wang L (2009) Electroanalysis 21(13):1521–1528
4. Yang P, Wei W, Tao C, Zeng J (2007) Bull Environ Contam Toxicol 79:5–10
5. Zhang D, Deng Y, Qi H, Gao Q, Zhang C (2009) Sensors Actuators B Chem 136:113–121
6. Xu M, Cui JL, Han R, Ai S (2012) J Solid State Electrochem 16:2547–2554
7. Hashemnia S, Khayatzadeh S, Hashemnia M (2012) J Solid State Electrochem 16:473–479
8. Ziyatdinova G, Gainetdinova A, Morozov M, Budnikov H, Grazhulene S, Red'kin A (2012) J Solid State Electrochem 16:127–134
9. Kheiri F, Sabzi RE, Jannatdoust E, Sedgui H (2011) J Solid State Electrochem 15:2593–2599
10. Liu X, Li X, Liu Y, Zeng X, Kong B, Luo S, Wei W (2012) J Solid State Electrochem 16:833–889
11. Wang L, Zhang Y, Du Y, Lu D, Zhang Y, Wang C (2012) J Solid State Electrochem 16:1323–1331
12. Yin H, Zhang Q, Zhou Y, Ma Q, Liu T, Zhu L, Ai S (2011) Electrochim Acta 56(6):2748–2753
13. Thelander C, Agarwal P, Brongersma S, Eymery J, Feiner LF, Forchel A, Scheffler M, Riess W, Ohlsson BJ, Gösele U, Samuelson L (2006) Mater Today 9:28–35
14. Davies TJ, Bank SCE, Compton RG (2005) J Solid State Electrochem 9:797–808
15. Ghanem MA (2007) Electrochem Comm 9:2501–2506
16. Laberty-Robert C, Kuemmel M, Allouche J, Boissière C, Nicole L, Grosso D, Sanchez C (2008) J Mater Chem 18:1216–1221
17. Kuemmel M, Allouche J, Nicole L, Boissière C, Laberty-Robert C, Amenistcsch H, Sanchez C, Grosso D (2007) Chem Mater 19:3717–3725
18. Kuemmel M, Boissière C, Nicole L, Laberty-Robert C, Sanchez C, Grosso D (2008) J Sol-gel Sci Technol 48:102–112
19. Lantiat D, Vivier V, Grosso D, Laberty-Robert C, Sanchez C (2010) Chem Phys Chem 11(9):1971–1977
20. Mosa J, Fontaine O, Ferreira P, Borges RP, Vivier V, Grosso D, Laberty-Robert C, Sanchez C (2011) Electrochim Acta 56: 7155–7162
21. Fontaine O, Laberty-Robert C, Sanchez C (2012) Langmuir 28 (7):3650–3657
22. Walcarius A (2010) Anal Bional Chem 396:261–272
23. Khoo SB, Zh J (1999) Electroanalysis 11(8):546–552
24. Sun Y, Chen J, Li A, Liu F, Zhang Q (2005) React Funct Polym 64:63–73
25. Davis J, Vaugham DH, Cordosi MF (1998) Electrochim Acta 43 (3–4):291–300
26. Teichert C (2002) Physics Reports Rev Sect Phys Lett 365: 335–432
27. Doblhofer K (1994) Thin polymer film on electrodes: A physico-chemical approach, in electrochemistry of novel materials. VCH, New York
28. Brown B, Aaron M (2001) In: Smith J (ed) The rise of modern genomics, 3rd edn. New York, Wiley
29. Rhodes CP, Long JW, Doescher MS, Dening BM, Rolinson DR (2004) J Non-Cryst Solids 350:73–79
30. Long JW, Rolinson DR (2007) Acc Chem Res 40(9): 854–862
31. McEvoy TM, Long JW, Smith TJ, Stevenson KJ (2006) Langmuir 22:4462–4466
32. Nasr B, Abdellatif G, Cañizares P, Sáez C, Lobato J, Rodrigo MA (2005) Environ Sci Technol 39(18):7234–7239
33. Stretiweiser A, Heathcock CH, Kosower EM (1992) Introduction to organic chemistry, 4th edn. MacMillan, New York
34. Cai Q, Khoo SB (1994) Anal Chem 66:4543–4550
35. Qian G, Yang C, Pu W, Huang J, Zhang J (2007) Synth Met 157 (10–12):448–453
36. Nematollahi D, Rahchamani R (2002) Tetrahedron Lett 43: 147–150
37. Araña J, Fernández Rodríguez C, González Díaz O, Herrera Melián JA, Pérez Peña J (2005) Catal Today 101:261–266
38. Rincón AG, Pulgarin C, Adler N, Peringer P (2001) J Photochem Photobiol A: Chem 139:233–241
39. Montilla F, Cotarelo MA, Morallón E (2009) J Mater Chem 19:305–310
40. Martin ST, Kesselman JM, Park DS, Lewis NS, Hoffman MR (1996) Environ Sci Technol 30:2535–2542
41. Lunsford SK, Choi H, Stinson J, Yeary A, Dionysiou DD (2007) Talanta 73:172–177
42. Rodríguez R, Blesa MA, Regazzoni AE (1996) J Colloid Interface Sci 177:122–131

43. Araña J, Rodríguez López VM, Pulido Melián E, Suárez Reyes MI, Doña Rodríguez JM, González Díaz O (2007) Catal Today 129(1-2):177–184
44. Elliot JM, Attard GS, Bartlett PN, Coleman NRB, Merckel DAS, Owen JR (1999) Chem Mater 11:3602–3609
45. Araña J, Pulido Melián E, Rodríguez López VM, Peña Alonso A, Doña JM (2007) J Hazardous Mat 146:520–528
46. Wang SG, Li YQ, Zhao XJ, Wang JH, Han JJ, Wang T (2007) Relat Mater 16:248–252
47. Yu J, Du W, Zhao F, Zeng BZ (2009) Electrochim Acta 54: 984–988
48. Yang P, Wei W, Yang L (2007) Microchim Acta 157:229–235
49. Qi H, Zhang C (2005) Electroanalysis 17:832–838
50. Wang Z, Li S, Lv Q (2007) Sens Actuators B 127:420–425
51. Carvalho RM, Mello C, Kubota LT (2000) Anal Chim Acta 420:109–121
52. Zhang X, Duan S, Xu X, Xu S, Zhou C (2011) Electrochim Acta 56:1981–1987